Simulation of Optical Microfiber Strain Sensors Based on Four-Wave Mixing

Shi-Han Tang, Zhen-Xing Wu, Fei Xu, and Yan-Qing Lu

***Abstract*— We investigate the performance of a microfiber strain sensor based on the nonlinear four-wave mixing process. This simple sensor of only an elliptical microfiber has considerable advantages, such as sensing directly by microfiber inherent nonlinearity in the telecommunication range and being compatible with the existing fiber network. Dispersion, nonlinearity, and strain effect are analyzed to find optimum sensing performance. The numerical simulations reveal that the strain can cause a marked wavelength shift of the signal wave. The wavelength shift range can be more than 74 nm within a reasonable strain range. To the ultimate strain range of 30 mε, the average strain sensitivity of 2.46 pm/$\mu\varepsilon$ can be obtained when the pump wavelength is 1550 nm and the peak power is 100 W. In addition to the range of 5 mε, it could achieve 9.86 pm/$\mu\varepsilon$ by optimizing the fiber size and highly birefringent characteristic. This strain sensor with high sensitivity, simple configuration, light, and portable performance has wide applications in mechanical detection and fault diagnosis and is of intensified interest for a great deal of wavelength selected devices in quantum information process.**

***Index Terms*— Four-wave mixing, optical fiber sensors, strain.**

I. Introduction

SINCE the advantages over conventional electrical sensors, fiber-optic sensors have attracted much attention and developed in various physical and chemical sensing fields like strain [1], temperature [2], gas [3], and magnetic field [4]. In recent years, optical strain sensors have been significant in strain measurements. To seek higher sensitivity, higher precision, better repeatability, and simpler configuration, much efforts have been made to improve the performance of strain sensors based on linear optical response such as fiber Bragg gratings (FBGs), Mach-Zehnder (M-Z) interferometers, and long period gratings (LPGs) [5]–[8]. A sensitivity of as high as 7.6 pm/$\mu\varepsilon$ under 4 mε has been reported in Ref [8] by the LPG. However, all LPGs, FBGs and M-Z interferometers entail complicated sensing structures [5]–[8]; and both of LPGs and FBGs have other problems of intricate fabrication and fragile feature.

The nonlinear optical sensors have their own advantages: simple configuration, use of inherent nonlinearity and no complicated post-processing, such as the grating writing. Among the nonlinear processes, Four-wave mixing (FWM) is one kind of the important third-order nonlinear process in optical fibers, which has applications as signal amplifiers [9], and wavelength converters [10]. Further investigations demonstrate the significant degenerate FWM [11]. And they extend applications in sensors [12], lasers [13], supercontinuum sources [14], and even quantum communications [15]. It is well known FWM is sensitive to weak variation of the group-velocity dispersion (GVD) profile. By detecting the Stokes and Anti-Stokes frequency shifts, FWM optical sensors have been demonstrated to achieve highly sensitive label-free selective biosensing [16] and strain sensing [17] in MOFs. However, the applications in the conventional fibers are limited by the dispersion characteristics. Recently, optical microfibers have attracted growing interest with the development of computer-controllable tapering rig. Fabricated by heating and tapering a conventional single-mode fiber (SMF), an optical microfiber with a circular or elliptical cross-section and a sub-wavelength diameter can offer a large evanescence field, a tight optical confinement, and in particular, a flexible GVD profile. The GVD profile is diameter-dependent and can be finely tuned with a large tuning range by tapering the microfiber. Zero-dispersion wavelength (ZDW) can shift 270 nm when tapering the single mode fiber (SMF) from 5 μm to 2 μm. Further tapering to 1 μm, the dispersion curve has substantial change and the relation between the dispersion and the wavelength is not monotonic function from 600 nm to 1550 nm. Two ZDWs appear in 650 nm and 1344 nm for the 1μm-diameter microfiber, as a contrast to one ZDW for the 2μm-diameter microfiber. Hence, optical microfibers should have the great potential in FWM optical strain sensors.

In this paper, we investigate the performance of the strain sensor based on FWM in optical circular or elliptical microfibers. Our calculation shows the GVD profiles and FWM wavelengths of microfibers are sensitive to external strain, and an average strain sensitivity of as high as 2.46 pm/$\mu\varepsilon$ can be achieved with the ultimate strain range of 30 mε. By optimizing the diameter to near 1.61μm, an average strain sensitivity of 9.86 pm/$\mu\varepsilon$ can be achieved with the ultimate strain range of 5 mε, which is much larger than the previous investigation.

Compared with expensive MOFs, optical microfibers are easy to be fabricated and connected with the low cost. The sensor based on the microfiber has higher average sensitivity, simpler configuration. Moreover, the large strain-induced shift is applicable to a number of wavelength selected devices,

Manuscript received January 14, 2016; revised February 8, 2016; accepted February 12, 2016. Date of publication February 25, 2016; date of current version March 16, 2016. This work was supported in part by the National 973 Program under Grant 2012CB921803 and in part by the National and Natural Science Foundation of China under Grant 61322503, Grant 61225026, Grant 61490714, and Grant 61475069. The associate editor coordinating the review of this paper and approving it for publication was Prof. Yu-Cheng Lin.

The authors are with the National Laboratory of Solid State Microstructures, College of Engineering and Applied Science, Nanjing University, Nanjing 210093, China (e-mail: 15298387590@163.com; 15996224511@163.com; feixu@nju.edu.cn; yqlu@nju.edu.cn).

Digital Object Identifier 10.1109/JSEN.2016.2530681

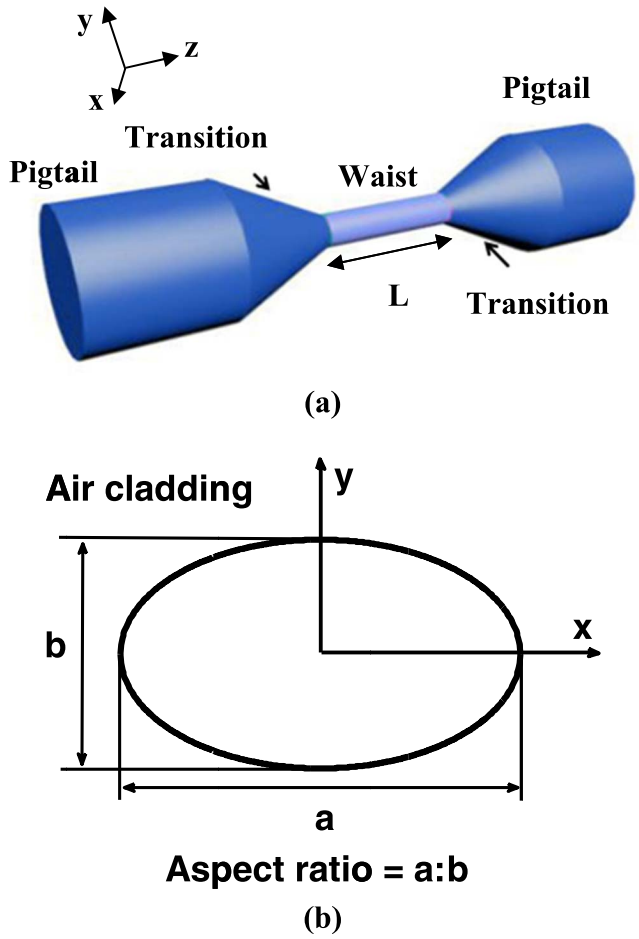

Fig. 1. (a) The schematic of the microfiber. (b) The model of an air-cladding elliptical microfiber, x-axis represents the long-axis direction, y-axis represents the short-axis direction.

for example, a tunable laser or a wavelength-tuning entangled photon source.

II. Theoretical Model

Generally, a microfiber tapered from the conventional SMF has a circular cross-section, and it is typically not highly-birefringent (Hi-Bi). Recently, elliptical microfibers with high birefringence have been demonstrated experimentally by tapering a rectangle cladding fiber or an asymmetrical SMF [18], [19]. In fact, a circular microfiber could be seen as a special case of the elliptical microfiber with an aspect ratio of 1. Figure 1 (a) is an illustrative diagram of the microfiber. The L represents the length of the waist. The z-axis is the direction of the wave transmission direction. The x-y plane is perpendicular to the transmission direction. And Fig. 1 (b) is the sectional view of the waist of the microfiber. The theoretical model is used to study the strain properties of the air/cladding microfibers. The model comprises two layers or regions: an infinite air-cladding and an elliptical silica core. Here the long-axis diameter is a and the short-axis diameter is b, respectively. We mainly optimize the sensitivity by tuning a and b.

Pigtails of the microfiber strain sensor make it easy to be compatible with the current fiber network and use the fiber devices. With regard to the length (L) of the microfiber, we should increase the L to add the signal gain, and L=15 cm is a common choice in experiments [20].

FWM occurs when two high-power pump waves are launched into a fiber, giving rise to two new waves (known as a signal and an idler), the wavelengths of which do not coincide with any of the others. This process simultaneously generates the signal photon and the idler photon at new frequencies ω_s and ω_i when two strong pumping photons ω_{p1} and ω_{p2} are annihilated. This third-order nonlinear process FWM satisfies energy and momentum conversation laws as

$$\omega_{p1} + \omega_{p2} = \omega_s + \omega_i. \tag{1}$$

In the degenerate case, $\omega_{p1} = \omega_{p2}$, thus the equation should be simplified as

$$2\omega_p = \omega_s + \omega_i. \tag{2}$$

From the approximate solution of coupled amplitude equations [21], the significant FWM phenomenon should satisfy the phase-matching condition $\kappa = 0$, where the effective phase mismatch κ is related to the nonlinear coefficient γ and the peak power of the pump laser P

$$\kappa = \Delta k + 2\gamma P, \tag{3}$$

wherein Δk is taken to describe the mismatch of propagation constants

$$\Delta k = (n_s\omega_s + n_i\omega_i - 2n_p\omega_p)/c. \tag{4}$$

The parametric gain will be maximized when $\kappa = 0$ or $\Delta k = -2\gamma P$ is satisfied. Hence the GVD profile of the microfiber is crucial for the significant FWM phenomenon.

When an external force is applied parallel to the microfiber, the mechanical strain stretches the microfiber not only to change the diameter according to the volume conservation, but also to change the refractive index according to elasto-optic effect [22], [23].

$$\begin{aligned} d_x &= d_{0x}/(1+\varepsilon)^{1/2} \\ d_y &= d_{0y}/(1+\varepsilon)^{1/2} \\ n_x &= n_{0x} - n_{0x}^3[p_{12} - \sigma(p_{11}+p_{12})]\varepsilon/2 \\ n_y &= n_{0y} - n_{0y}^3[p_{12} - \sigma(p_{11}+p_{12})]\varepsilon/2, \end{aligned} \tag{5}$$

where the subscripts 0, x or y indicate the initial condition and the x- or y- axis directions respectively in silica fibers, the Poisson's radio $\sigma = 0.25$, and the strain-optic coefficients $p_{11} = 0.120$, $p_{12} = 0.27$ [23]. The effective refractive index n_{eff} and GVD profile will change with the strain, then the phase-matching FWM wavelengths will shift. The relation between strain and FWM process is a principal presentation of the average sensitivity of the FWM strain sensor. The strength of glass nanowires can be as high as 10 GPa as reported [24], here we choose a reasonable strain range of 30 mε in our simulation.

Moreover, because of the birefringence of the elliptical microfiber, we have to distinguish different polarizations. In our simulation, the four involved waves are expected to maintain the same polarization which has the largest efficiency.

III. Strain Induced Performance Chance

A. Dispersion

The dispersion of the microfiber is vital to the phase-matching condition of FWM and it is evaluated as [21]

$$D(\lambda) = -\frac{\lambda}{c}\frac{d^2 n_{eff}}{d\lambda^2}, \tag{6}$$

where λ is the wavelength, c is the velocity of the light in vacuum. The material dispersion given by Sellmeier's formula is directly included in the calculation. To generate FWM efficiently, it is required that the pump wavelength coincides with the fiber ZDW. Here we assume the pumping wavelength is near 1550 nm, and we have to optimize the fiber size to achieve the ZDW around the pumping wavelength. During the simulation of the dispersion, only the x-polarization fundamental mode is considered.

Figure 2 shows the dispersion profiles from 1400 nm to 1600 nm for different microfiber diameters and strains. A marked dispersion shift between adjacent curves is observed in Fig. 2. Without the strain, the dispersion curve with the larger long-axis diameter is much flatter than the others as it shows in Fig. 2 (a). Decrease of the long-axis diameter makes the dispersion decrease. Further decrease of the long-axis diameter to 1.5 μm brings in the ZDW near 1550 nm. For a FWM strain sensor, the dispersion profile also can significantly decrease when the applied strain increases as it shows in Fig. 2 (b), along with the near-1550nm ZDW in the 30mε line. A 40 ps/km/nm difference of the dispersion can be obtained when the strain is tuned from 0 mε to 30 mε.

According to the analysis above, we can figure out that the elliptical microfibers with the long-axis diameter from 1.5 μm to 1.55 μm exhibit an excellent FWM-sensing condition. The results help us find the optimum parameters of the FWM strain sensor.

B. Nonlinear Coefficient

Another important parameter of FWM strain sensors is the nonlinear coefficient (γ). It not only affects the phase-matching condition, but also leads to the change of the parametric gain (g). The use of micro-scale structure has the considerable advantage to achieve large γ easily. If the phase-matching condition $\kappa = 0$ is satisfied, the maximum parametric gain is $g_{max} = \gamma P$.

Where γ is related to the mode field distribution of the wave and the material of the waveguide [25]

$$\gamma = \frac{k(\frac{\varepsilon_0}{\mu_0}) \int n_2(x,y) n^2(x,y)[2|\mathbf{e}|^4 + |\mathbf{e}^2|^2]dA}{3\left|\int (\mathbf{e}\times\mathbf{h}^*)\cdot\hat{z}dA\right|^2}, \tag{7}$$

where k is the wave vector, **e** is the electric field, and **h** is the magnetic field. These parameters are calculated by the finite element method. The ε_0, μ_0, n_2 are constants that represent the electric permittivity, the magnetic permeability in vacuum, and the nonlinear index coefficient respectively. Here $n_2 = 2.6\times10^{-20}$m^2/W for silica [25] and 5.0×10^{-23}m^2/W for air [26].

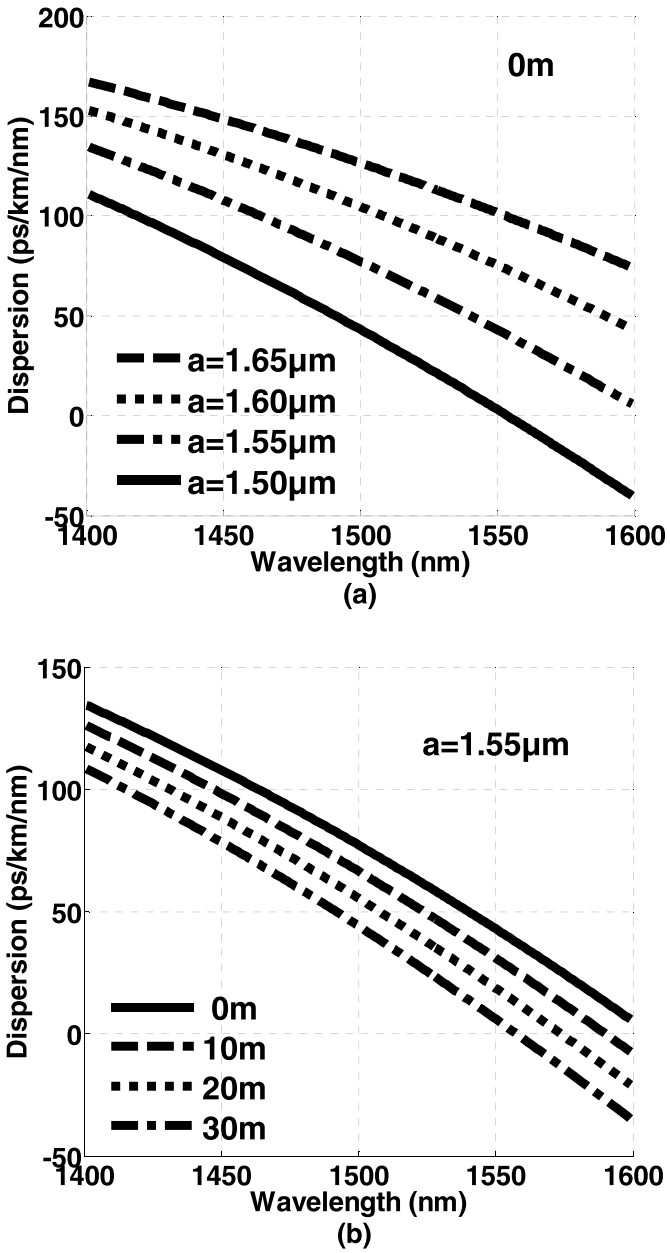

Fig. 2. (a) The dispersion profiles of x-polarized fundamental mode with different elliptical microfiber's long-axis diameters without the strain. (b) The dispersion profiles with different strains when a=1.55μm. Here the aspect ratio=3:2.

Fig. 3 (a) shows the γ at different long-axis diameters without the strain. The change of the fiber diameter and the mode field distribution lead to the obvious variation of γ. The γ increases by decreasing the long-axis diameter and the elliptical microfibers' γ is much larger ($\sim$ 60 times) than the SMFs' under the same condition. This advantage allows series of nonlinear applications, e.g., wavelength conversion, phase-locked laser through filamentation, tunable optical probe [27]–[29].

Fig. 3 (b) shows the effect of the strain, which is not significant compared with the effect of long-axis diameters. The γ of the elliptical microfiber at 1550nm is found to be around 0.11 m^{-1}W^{-1} and the strain-induced variation $\Delta\gamma$ is

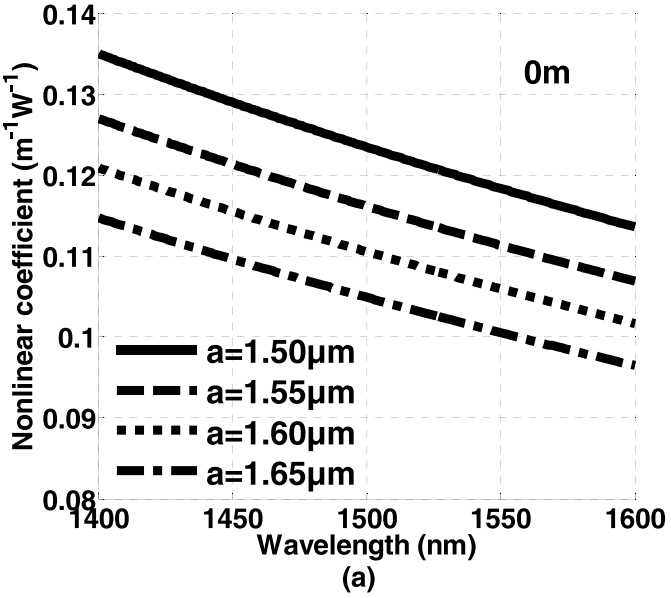

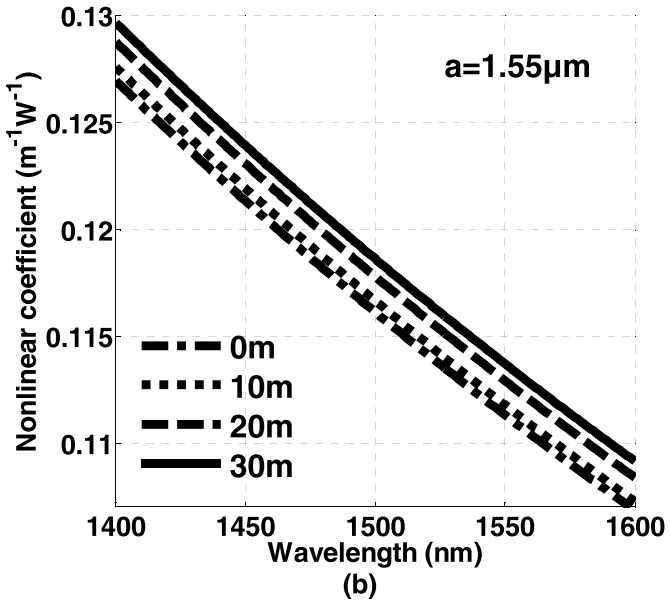

Fig. 3. (a) The nonlinear coefficient with different elliptical microfiber's long-axis diameters without the strain. (b) The nonlinear coefficient with different strains when a=1.55 μm. Here the aspect ratio=3:2.

very small. It indicates that we can set γ as a constant in the simulation of a FWM strain sensor.

C. Strain-Induced FWM Shift

The simulation results above show that elliptical microfibers with the long-axis diameter near 1.55 μm are promising for FWM strain sensors. The nearly-zero dispersion and large nonlinearity would enable a great tuning of signal (idler) wavelength by the strain. The strain-induced shift of the signal (idler) wavelength can be calculated from the phase-matching condition and elasto-optic effect, according to Eqs. (3) - (5). The shift $\Delta\lambda$ of the signal wavelength is illustrated with Fig. 4, with a given pump wavelength of 1550 nm,

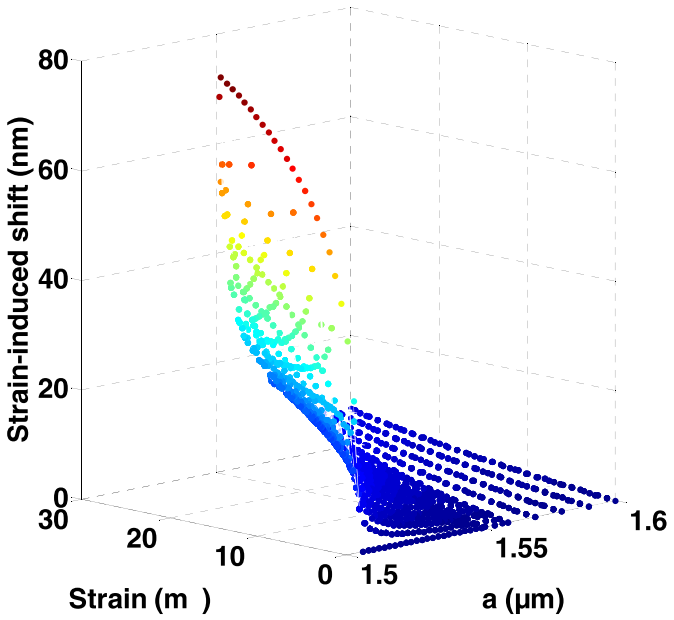

Fig. 4. 3D graphs of strain-induced shift as a function of the fiber long-axis diameter and the strain of the elliptical microfiber at the aspect ratio=3:2, λ = 1550 nm and P = 100 W.

a peak power of 100 W and an aspect ratio of 3:2. It increases with smaller long-axis diameter or larger strain as expected. There is an optimum diameter for the highest average sensitivity when the ultimate strain range is 30 mε. Here we still only consider the case that all waves maintain the x-axis polarization.

The tensile strain causes the ZDW blue shift just as the Fig. 2 (b) shows. When the pump wavelength is fixed, the increase of the tensile strain moves the pump wavelength from the anomalous dispersion to the normal dispersion towards a certain point of fiber parameters. So the phase-matching condition could not be satisfied or only satisfied with larger frequency shift, which results in the discontinuous change.

The strain presents a significant effect on the FWM signal (idler) wavelength for the smaller elliptical microfiber. For the long-axis diameter above 1.55 μm, the strain-induced shift is limited by the fiber strain limit 30 mε. Phase-matching condition is satisfied over the total range from 0 to 30 mε; for a = 1.55 μm, the strain induces the largest wavelength shift of the signal and the highest average sensitivity of the sensor within the ultimate strain range of 30 mε. When the diameter is below 1.55μm, the maximum shift can only achieved when the ultimate strain is the largest strain which is satisfied with the phase-matching condition. The largest strain is smaller and smaller when the long-axis diameter is decreasing from 1.55 μm. Until the diameter of 1.5 μm, the largest strain which is satisfied with the phase-matching condition is near 0.

Fig. 4 indicates the reduced long-axis diameter at a given strain leads to the larger strain-induced shift; alternatively, for a fixed long-axis diameter, one could increase the shift by amplifying the strain. Thus for the aspect ratio 3:2 used here, the maximum shift of the signal is 72.35 nm within 30 mε, which is almost 700 times more than the SMF

TABLE I
SUMMARIZATION OF THE MAXIMUM STRAIN-INDUCED SHIFT IN FIG.5

Aspect Ratio	X-Polarization (nm)	Y-Polarization (nm)
1:1	67.74	67.74
5:4	69.14	67.69
3:2	72.35	67.5
5:3	73.71	66.63

(its shift is less than 0.1 nm) on the similar condition. The micro-scale structure is beneficial for the FWM strain sensor. The average sensitivity of 2.42 pm/$\mu\varepsilon$ is achieved when a = 1.55 μm within 30 mε and the average sensitivity would be optimized further when a smaller strain range is permitted. Considering the strain range of 5 mε, the highest average sensitivity of 9.72 pm/$\mu\varepsilon$ occurs when a = 1.512 μm.

D. Optimization

The average sensitivity and the strain range of a FWM strain sensor based on an elliptical microfiber have been obtained above when the aspect ratio is 3:2. They can be improved by further optimization of Hi-Bi characteristic at the same pump wavelength and power (1550nm, 100W).

As shown in Fig. 5, each subgraph is virtually identical to be divided into two sections: a rising edge and a falling edge. Each point on the falling edge achieves the maximum shift when the ultimate strain is 30 mε. Each point on the rising edge achieves the maximum shift when the ultimate strain is the largest strain which is satisfied with the phase-matching condition. The tensile strain causes the ZDW shift and results in the discontinuous change. The largest strain is smaller and smaller when the long-axis diameter is decreasing from the turning point. As a result, the maximum shift is decreasing when the long-axis diameter is decreasing from the turning point. In these subgraphs, we are easy to pick out the optimum fiber parameters (the turning point).

The maximum shifts as a function of the long-axis diameter at the several different aspect ratios and polarization states are shown in Fig. 5. For the aspect ratio of 1, we only need consider a polarization state.

We analyze the data to optimize the average sensitivity of the sensors within the ultimate strain range of 30 mε. The highest average sensitivity within 30mε of a certain aspect ratio can be gained from the turning point on the graph. The analysis of the rising edge will assist us to optimize the average sensitivity under a smaller strain range. The maximum average sensitivities corresponding to the ultimate strain range of 5 mε are studied. When the long-axis diameter is near 1.61 μm, and the a/b ratio is 5:3, the average sensitivity could be as high as 9.86 pm/$\mu\varepsilon$, which is much higher than Gu's theoretical result (4.46 pm/$\mu\varepsilon$) [17]. With the average sensitivity up to 9.86 pm/$\mu\varepsilon$, it is capable of accomplishing the requirements for weak signal sensing.

Comparisons of the turning points are shown in Table I to find more optimum parameters to sensors of the 30 mε ultimate strain range. Table I presents the largest strain-induced

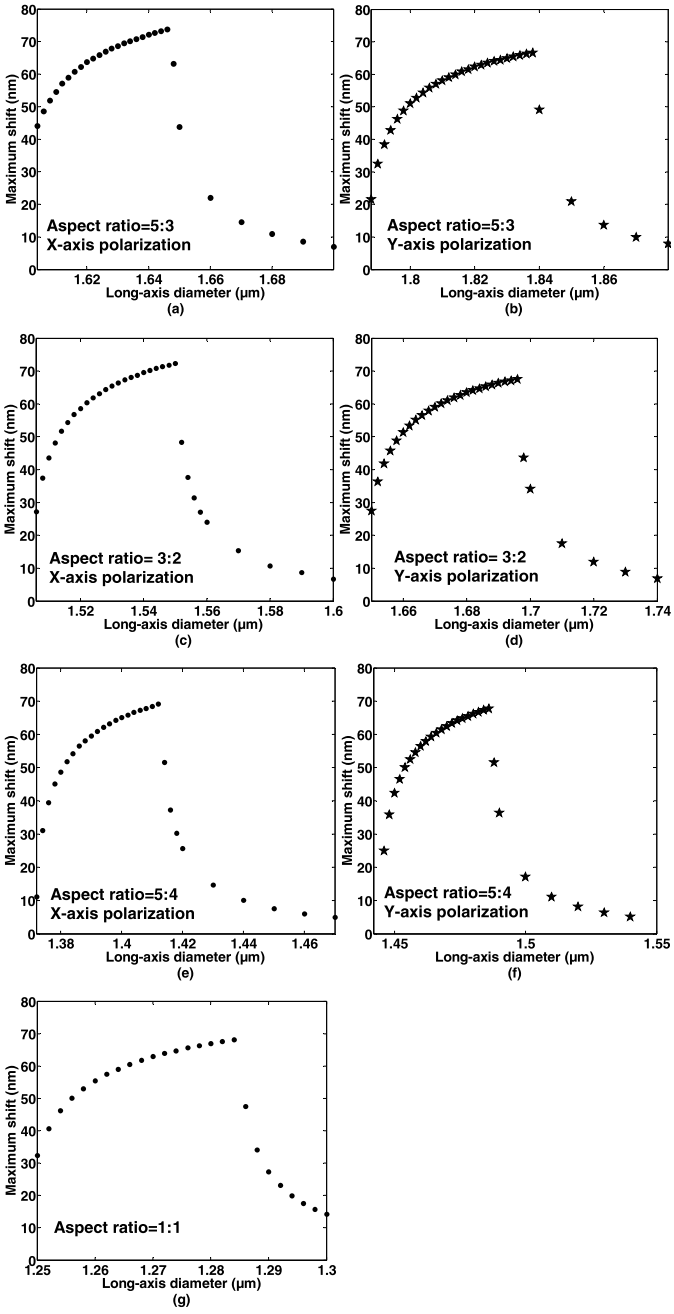

Fig. 5. The maximum strain-induced FWM shift in the elliptical microfibers with different aspect ratios: (a) and (b) 5:3, (c) and (d) 3:2, (e) and (f) 5:4, (g) 1:1 with different polarization fundamental modes. Here λ = 1550 nm, P = 100 W, the strain range is 30 mε.

shift of the signal under various aspect ratios and polarizations. The results show that the Hi-Bi is a promising alternative to improve the strain sensor performance. However, it also entails a correct x-polarization. The maximum shift changes little for y-polarization. A maximum shift above 73.71 nm appears when the aspect ratio is 5:3 and the high average strain sensitivity of 2.46 pm/$\mu\varepsilon$ is achieved within 30mε. Such a large strain-induced shift will give a promising development of some wavelength selected devices. The maximum strain-induced shift of the signal wave for a 5:3 elliptical microfiber is 6 nm larger than that for a circular microfiber, moreover,

$\sim$0.2 pm/$\mu\varepsilon$ larger in the sensitivity. Meanwhile the Hi-Bi configuration allows a further optimization, such as introducing some strain-sensitive Hi-Bi structure as slot-microfibers. Hi-Bi configuration allows more than 4 types phase-matching condition [21] due to the different polarization directions of the involved four waves. It could satisfy in both the anomalous and normal dispersion. The FWM strain sensor's performance could improve further by bringing in different polarization directions among four waves. Because the strain could change the birefringence and the frequency shift would wide-range change.

Meanwhile the temperature problem is an important influence factor of the majority of the optical fiber sensors. Here the phase-matching condition will be changed. The general solution is using an extra device as a reference to achieve temperature compensation which will be achieved by further signal processing.

As for the FWM sensor, the paper [17] has shown that the sensing process is near linear within a relative small strain range. To our proposed sensor, it is also applicable when the strain range is small. Even though we choose the larger range such as 30 mε, we could calculate the best curve fitting to the signal response to complete the sensing process.

The reproducibility of the sensor is related to the fabrication reproducibility of the microfibers' diameters and high-birefringent characteristic. Along with the development of computer-controllable tapering rig, the reproducibility of the microfiber strain sensor can be enhanced greatly. The resolution also could be optimized by using a narrow-linewidth pump laser and a long and uniform microfiber.

IV. Conclusion

In this paper, a nonlinear strain sensor based on an elliptical microfiber with simple configuration, small size, and high sensitivity is investigated. This device has the natural advantages to be compatible with the existing transmission technology. The simulation results present that the strain sensor could has a high strain average sensitivity of 2.46 pm/$\mu\varepsilon$ to 30mε and 9.86 pm/$\mu\varepsilon$ to 5 mε by optimizing the microfiber geometry at the pumping peak power of 100 W. This is more than four times higher than the sensitivity of MOF sensors [12], [17], [30], [31], and hundreds of times higher than the SMF sensors. It provides better performance in sensing, such as fault diagnosis and mechanical detection. What is more, the large strain-induced shift will give further insight towards applications of wavelength selected devices such as a wavelength-tuning entangled photon source.

References

[1] W. Luo, J.-L. Kou, Y. Chen, F. Xu, and Y.-Q. Lu, "Ultra-highly sensitive surface-corrugated microfiber Bragg grating force sensor," *Appl. Phys. Lett.*, vol. 101, no. 13, p. 133502, Sep. 2012.

[2] S.-J. Qiu, Y. Chen, F. Xu, and Y.-Q. Lu, "Temperature sensor based on an isopropanol-sealed photonic crystal fiber in-line interferometer with enhanced refractive index sensitivity," *Opt. Lett.*, vol. 37, pp. 863–865, Mar. 2012.

[3] F. Zhou, S.-J. Qiu, W. Luo, F. Xu, and Y.-Q. Lu, "An all-fiber reflective hydrogen sensor based on a photonic crystal fiber in-line interferometer," *IEEE Sensors J.*, vol. 14, no. 4, pp. 1133–1136, Apr. 2014.

[4] S.-J. Qiu, Q. Liu, F. Xu, and Y.-Q. Lu, "Ampere force based photonic crystal fiber magnetic field sensor," *Sens. Actuators A, Phys.*, vol. 210, pp. 95–98, Apr. 2014.

[5] J.-L. Kou, M. Ding, J. Feng, Y.-Q. Lu, F. Xu, and G. Brambilla, "Microfiber-based Bragg gratings for sensing applications: A review," *Sensors*, vol. 12, pp. 8861–8876, Jul. 2012.

[6] T. Mizunami, T. Mori, and T. Fujiyoshi, "Highly strain-sensitive long-period grating in Hi-Bi fiber with a reference fiber Bragg grating," in *Proc. Adv. Photon. Congr.*, 2012, p. JTu5A.49.

[7] W. Shin, Y. L. Lee, B.-A. Yu, Y. C. Noh, and T. J. Ahn, "Highly sensitive strain and bending sensor based on a fiber Mach–Zehnder interferometer in photonic crystal fiber," in *Proc. Conf. Lasers Electro-Opt.*, May 2010, pp. 1–2.

[8] Y.-P. Wang, L. Xiao, D. N. Wang, and W. Jin, "Highly sensitive long-period fiber-grating strain sensor with low temperature sensitivity," *Opt. Lett.*, vol. 31, no. 23, pp. 3414–3416, 2006.

[9] W. Xie, I. Fsaifes, T. Labidi, and F. Bretenaker, "Investigation of degenerate dual-pump phase sensitive amplifier using multi-wave model," *Opt. Exp.*, vol. 23, pp. 31896–31907, Dec. 2015.

[10] H.-J. Kim, J.-I. Song, and H.-J. Song, "An all-optical frequency up-converter utilizing four-wave mixing in a semiconductor optical amplifier for sub-carrier multiplexed radio-over-fiber applications," *Opt. Exp.*, vol. 15, pp. 3384–3389, Mar. 2007.

[11] M. H. Frosz, A. Stefani, and O. Bang, "Highly sensitive and simple method for refractive index sensing of liquids in microstructured optical fibers using four-wave mixing," *Opt. Exp.*, vol. 19, no. 11, pp. 10471–10484, May 2011.

[12] H. F. Martins, M. B. Marques, and O. Frazão, "Temperature-insensitive strain sensor based on four-wave mixing using Raman fiber Bragg grating laser sensor with cooperative Rayleigh scattering," *Appl. Phys. B*, vol. 104, pp. 957–960, Sep. 2011.

[13] T. Huang *et al.*, "All-fiber multiwavelength thulium-doped laser assisted by four-wave mixing in highly germania-doped fiber," *Opt. Exp.*, vol. 23, pp. 340–348, Jan. 2015.

[14] P. M. Moselund, M. H. Frosz, C. L. Thomsen, and O. Bang, "Back-seeding of higher order gain processes in picosecond supercontinuum generation," *Opt. Exp.*, vol. 16, pp. 11954–11968, Aug. 2008.

[15] X. Li, C. Liang, K. F. Lee, J. Chen, P. L. Voss, and P. Kumar, "Integrable optical-fiber source of polarization-entangled photon pairs in the telecom band," *Phys. Rev. A*, vol. 73, p. 052301, May 2006.

[16] J. R. Ott, M. Heuck, C. Agger, P. D. Rasmussen, and O. Bang, "Label-free and selective nonlinear fiber-optical biosensing," *Opt. Exp.*, vol. 16, no. 25, pp. 20834–20847, Dec. 2008.

[17] B. Gu, W. Yuan, M. H. Frosz, A. P. Zhang, S. He, and O. Bang, "Nonlinear fiber-optic strain sensor based on four-wave mixing in microstructured optical fiber," *Opt. Lett.*, vol. 37, pp. 794–796, Mar. 2012.

[18] Y. Jung, G. Brambilla, K. Oh, and D. J. Richardson, "Highly birefringent silica microfiber," *Opt. Lett.*, vol. 35, pp. 378–380, Feb. 2010.

[19] H. Xuan, J. Ju, and W. Jin, "Highly birefringent optical microfibers," *Opt. Exp.*, vol. 18, pp. 3828–3839, Feb. 2010.

[20] L. Cui *et al.*, "Generation of correlated photon pairs in micro/nanofibers," *Opt. Lett.*, vol. 38, no. 23, pp. 5063–5066, 2013.

[21] G. P. Agrawal, "Four-wave mixing," in *Nonlinear Fiber Optics*, 4th ed. New York, NY, USA: Academic, 2007, pp. 368–423.

[22] A. Bertholds and R. Dandliker, "Determination of the individual strain-optic coefficients in single-mode optical fibres," *J. Lightw. Technol.*, vol. 6, no. 1, pp. 17–20, Jan. 1988.

[23] L. Yuan, "White-light interferometric fiber-optic strain sensor from three-peak-wavelength broadband LED source," *Appl. Opt.*, vol. 36, pp. 6246–6250, Sep. 1997.

[24] G. Brambilla and D. N. Payne, "The ultimate strength of glass silica nanowires," *Nano Lett.*, vol. 9, pp. 831–835, Feb. 2009.

[25] S. A. V and T. M. Monro, "A full vectorial model for pulse propagation in emerging waveguides with subwavelength structures part I: Kerr nonlinearity," *Opt. Exp.*, vol. 17, pp. 2298–2318, Feb. 2009.

[26] W. Guo, J.-L. Kou, F. Xu, and Y.-Q. Lu, "Ultra-flattened and low dispersion in engineered microfibers with highly efficient nonlinearity reduction," *Opt. Exp.*, vol. 19, pp. 15229–15235, Aug. 2011.

[27] M. H. Chou, I. Brener, M. M. Fejer, E. E. Chaban, and S. B. Christman, "1.5-μm-band wavelength conversion based on cascaded second-order nonlinearity in $LiNbO_3$ waveguides," *IEEE Photon. Technol. Lett.*, vol. 11, no. 6, pp. 653–655, Jun. 1999.

[28] C. P. Hauri *et al.*, "Generation of intense, carrier-envelope phase-locked few-cycle laser pulses through filamentation," *Appl. Phys. B*, vol. 79, pp. 673–677, Oct. 2004.

[29] Y. Nakayama *et al.*, "Tunable nanowire nonlinear optical probe," *Nature*, vol. 447, pp. 1098–1102, Jun. 2007.

[30] X. Dong, H. Y. Tam, and P. Shum, "Temperature-insensitive strain sensor with polarization-maintaining photonic crystal fiber based Sagnac interferometer," *Appl. Phys. Lett.*, vol. 90, p. 151113, Apr. 2007.
[31] T. K. Noh and Y. W. Lee, "Temperature-insensitive polarimetric fiber strain sensor with short polarization-maintaining photonic crystal fiber," *Appl. Phys. Exp.*, vol. 5, no. 11, p. 112502, Nov. 2012.

Shi-Han Tang received the bachelor's degree in material physics from Nanjing University, Nanjing, China, in 2013, where she is currently pursuing the master's degree with the College of Engineering and Applied Sciences. She is also with the National Laboratory of Solid State Microstructures, Nanjing University.

Zhen-Xing Wu received the bachelor's degree in material physics from Nanjing University, Nanjing, China, in 2014, where he is currently pursuing the master's degree with the College of Engineering and Applied Sciences. He is also with the National Laboratory of Solid State Microstructures, Nanjing University.

Fei Xu is currently a Professor with the College of Engineering and Applied Sciences, and the National Laboratory of Solid State Microstructures, Nanjing University, Nanjing, China. His current research interests include nonlinear optics and fiber optics.

Yan-Qing Lu is currently a Professor with the College of Engineering and Applied Sciences, and the National Laboratory of Solid State Microstructures, Nanjing University, Nanjing, China. His current research interests include nanophotonics and liquid crystal photonics.